Magnetorheological Fluid Flow in Microchannels

Joseph Whiteley

Faramarz Gordaninejad[1]
Professor
e-mail: faramarz@unr.edu

Xiaojie Wang
Research Assistant Professor

Department of Mechanical Engineering,
Composite and Intelligent Materials Laboratory,
University of Nevada,
Reno, NV 89557

This study presents experimental results on the flow of magnetorheological grease (MRG) through microchannels. MR materials flowing through microchannels create microvalves. The flow is controlled by injecting the MRG through microchannels with controlled adjustable rates. To study the effect of different channel diameters and surface roughnesses, microchannels made of stainless steel, PEEK, and fused silica materials with nominal internal diameters ranging from 1 mm to 0.075 mm (75 μm) are tested. A magnetic field is applied perpendicular to the microchannel flow and is controlled by an input electric current. The pressure drop of the flow is measured across the length of the microchannels. The dynamic pressure drop range and surface roughness effects are also discussed. The Herschel–Bulkley model for non-Newtonian fluid flow is employed to the experimental results with good agreement. The results show a significant pressure drop for different magnetic field strengths. [DOI: 10.1115/1.4000922]

1 Introduction

This study involves an experimental approach to characterize the flow behavior of magnetorheological (MR) suspensions in microchannels. Miniaturizing devices to the microscale and nanoscale levels is the current trend in many fields of study. The characteristics of fluid flow at the microlevel are not well understood. The applications that could benefit from devices involving microfluid flow are not yet fully realized. There has been limited research published on ER and MR fluid characteristics at the microscale level. When fully understood, this research could possibly be extended to applications in microfluidic sensors and valves, ranging from flow sensors and gas valves for gas pressure regulation, to complex microfluid handling systems for chemical analyses, consisting of pumps, valves, flow sensors, separation capillaries, control of structures, and systems using small devices, reactors for modification and separation of biological cells, energy systems such as mobile power sources, boundary layer control, coolers of macrodevices, and propulsion engines.

One possible application of this research is in magnetorheological fluid (MRF) microvalves. An advantage of a MRF microvalve is the fact that there are no moving parts within the valve mechanism. A similar type of valve has already been experimented with by researchers who have developed an electrorheological fluid (ERF) microvalve [1]. Since MRF has a higher yield stress than ERF, a MRF microvalve could be designed that is highly efficient as compared with an ERF one. Klein and Guckel [2] fabricated microcoils and microelectromagnets that can generate a magnetic field as much as 1 T in small gaps with an input coil power of 5 mW.

The behavior of field-controllable fluids in dampers and other devices at the macroscale have been well established [3]. With the recent technological advances, especially in microscale and nanoscale levels, many researchers have focused on understanding the behavior of fluids' flow at the microlevel. Papautsky et al. [4] summarized some preliminary research, which produced a variety of results that deviate from the theoretical value of 64 for the product of the friction factor and the Reynolds number (f Re).

The results from the experiments that have been conducted thus far are not consistent with each other. Experiments by Judy et al. [5] and Sharp and Adrian [6] have been carried out where liquid flow was studied in stainless steel and fused silica microchannels at a range of diameters from 15 μm to 250 μm with results indicating that there is no deviation from the conventional theory. The fluids that have been studied include water, oil, alcohol, and gas. Papautsky et al. [4] suggested that a deviation from conventional theory in these experiments may be related to measurement errors, including the measurements of microchannel diameter (D), microchannel length (L), pressure drop (ΔP), viscosity (μ), flow rate (Q), and surface effects.

Experimental studies of MR fluids at microscale level introduce a new arduous challenge. Because MRFs are suspensions of magnetically soft particles in liquids, such as, silicon oil or water, the flow behavior of MR fluid through microchannels is similar to a particle laden flow. Sharp and Adrian [6] have shown that with two phase particle laden flows, the ratio of the particle diameter to the channel diameter must be about 1:3 for clogging to occur. However, through the experiments that have been conducted in our studies with MR suspensions, this rule does not seem to hold true. Most theoretical studies of particle laden flow in microchannels do not take into account the effects of particle agglomeration, settling, and tubing diameter transitions that can result in clogging. This challenge is compounded further if the size of the iron particles is less than 100 nm. Kormann et al. [7] have shown that a nanobased MRF with 30 nm particle size exhibits an increase in shear yield stress under an applied magnetic field that is an order of magnitude smaller than that of a typical MR fluid.

Liu et al. [8] proposed that a biocompatible and biodegradable MRF may be an effective form of cancer treatment. A simulated blood network was created using silicone tubes with diameters ranging from 1.6 mm to 0.4 mm. MRFs were prepared using iron, iron oxide, and polystyrene embedded in iron oxide. The particle diameters ranged from 1.0 μm to 2.3 μm. Using human blood as the carrier fluid, the above particles were added so that the particle volume fractions ranged from 0.5% to 2.0%. A permanent magnet was used along a section of the tubing and the pressure drop was measured at different flow rates and magnetic field strengths. The results presented indicate that a pressure drop exceeding the 100 mmHg maximum, found in human arterioles, could be achieved. The pressure drops were sufficient enough to starve a cancer tumor by stopping the flow of blood to it.

The research by Haghgooie et al. [9] has shown that the columns formed by a MRF in microfluidic channels could be effective for DNA separation. The structure and dynamics of MRF with low particle volume fractions were analyzed to determine the ef-

[1]Corresponding author.

Contributed by the Applied Mechanics Division of ASME for publication in the JOURNAL OF APPLIED MECHANICS. Manuscript received June 27, 2009; final manuscript received December 10, 2009; published online April 14, 2010. Assoc. Editor: Nadine Aubry.

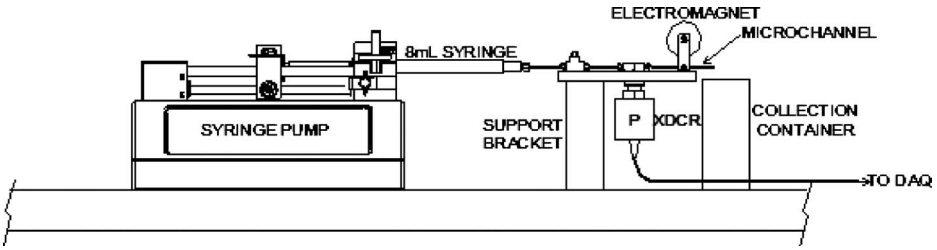

Fig. 1 Schematic of the experimental setup

fect of being constrained between two parallel plates. It was observed that the structure and dynamics of the colloids were highly dependent on the width of the channels.

This study focuses on the behavior of magnetorheological fluids flow through a microchannel. A special MRF, namely, MR grease, has been developed that will flow through a microchannel without clogging. The flow is controlled by injecting the MRF through the microchannel via a stainless steel syringe at a controlled adjustable rate. The pressure drop of the MRF flow is measured across the length of a tube with internal diameters ranging from 75 μm to 1 mm. A magnetic field is applied perpendicular to the microchannel MRG flow with a field strength ranging from 0 T to 0.56 T. Results are obtained for pressure drop as a function of applied magnetic field and flow rate.

2 Experimental Study

One of the major challenges in the proposed study is to develop a MR fluid (with high percentage of solid loading) that flows through microchannels and produce a significantly controllable pressure drop across the microchannel. Our preliminary results demonstrated that one can easily pass fluids with nanosized particles, such as ferrofluids, through microchannels. However, nanoparticles do not produce significant increase in pressure drop under an external magnetic field. In addition, when traditional MRFs were used, where the particle size is in the 1–10 μm range with large weight percentage of solid loadings, the flow through the microchannels would be plugged before any variation in pressure drop could be measured. It is clear that the successful MRF for this experiment has to have (a) micrometer size iron particles with high solids loadings, and (b) a base fluid that prevents these particles from settling or agglomeration at the entrance to or inside the microchannels resulting in blockage.

The first attempts in this effort involved using commercially available carbonyl iron micropowders in silicon oil or poly-alpha-olefin (PAO), with surfactants added to prevent particle agglomeration. None of these samples were able to flow through a 100 μm fused silica test microchannel. The next step was to synthesis iron oxide Fe_3O_4 particles similar to those found in ferrofluids, but with larger particle sizes. Several of these samples successfully flowed through the test microchannel with added polymer surface modifiers; however, because the particle size was still relatively small and the solids loading percentage in the fluid could not be increased above 10–20% without agglomeration occurring, the effect of the applied magnetic field on the yield stress was minimal.

A reverse micelle synthesis process was used to produce different phases of magnetic iron oxide nanoparticles. Heat treatment was used to control the phases of the iron oxide. Magnetic particle agglomerates with sizes averaging 200 nm were able to be produced by this process, and then, washed and added to hydraulic oil with a surfactant [10]. Unfortunately, the results were unsuccessful as microchannel blockage and insignificant MR effects from an applied magnetic field were observed.

A breakthrough came when a grease based carrier medium was used instead of the traditional oil. Commercially available grease was found to flow through microchannels, but when a large percentage of carbonyl iron powders were added, the resulting composition became too viscous to successfully flow through the microchannels. With the requirements of this study in mind, an experimental grease was synthesized that is able to accept the addition of large amounts of carbonyl iron powders while still maintaining its base viscosity. A summary of the composition of this base grease is as follows. Using PAO as carrier medium (83.3% weight of grease), modified smectite clay (12.6% by weight), and sorbitan monooleate (4% by weight) were added to the PAO and then mixed under a 500 rpm mixer for 1 h.

To prepare the MRG, the HQ series carbonyl iron powder (CIP) from BASF was mixed in with the base carrier grease. This CIP has an iron content greater than 97.5% and was selected based on its mechanical and geometric properties. The average particle diameter of the HQ powder is 1.1 μm, with 90% of the particles being less than 2.2 μm in diameter. This is roughly one-third of the size of the particle diameters of the powders used in commercial MRF today. The particles are also relatively hard in comparison to typical MRF carbonyl iron powders, which results in reduced particle breakdown and increased durability of the MRG.

The experimental setup to drive the MRF through microchannels requires some specialized fluid handling equipment that is typically only found in the biomedical industry. A schematic of the setup is shown in Fig. 1. A Harvard Apparatus PHD-4400 high pressure programmable syringe pump controls the flow of the MRF through the microchannel. Mounted in the pump is a Harvard Apparatus 8 ml or 2 ml stainless steel syringe, which dispenses the fluid from the syringe at a single or step changing flow rate.

At the exit of the syringe is a Swagelok fitting that connects a 5 cm length of 1.6 mm (1/16 in.) outside diameter (OD) stainless steel tubing to the syringe. At the end of that tubing is a stainless steel tee connected inline with port fittings. The tee is used to refill the syringe when all the MRG has been dispensed through the test section of the microchannel. After the tee, a second 5 cm length of the stainless steel tubing connects to a pressure gauge tee. The two pressure transducers used in this experiment are Cole Parmer models 68074-18 and 68074-20 with 3000 and 5000 psi (gauge) pressure ranges, respectively. All stainless steel tubing leading up to the pressure gauge tee has an internal diameter of 1 mm. The microchannel test sections are attached at the exit of the pressure gauge tee. Midway along the 5 cm length of microchannel, a controllable magnetic field is applied, with an electromagnet, to study the change in pressure drop when the field is applied. The electromagnet is constructed from silicone core iron with 1100 turns in the coil. The MRF exits the microchannel at atmospheric pressure and is collected in a container for reuse.

Three different tubing materials, with different surface roughness values, were used for the experiment to quantify the effect that the surface roughness had on the pressure drop across the microchannel test sections of the same nominal inside diameter (ID). Tubing used for the microchannel test sections varied between nominal IDs of 1 mm (1000 μm) and 0.075 mm (75 μm). Type 316 stainless steel and polyether ether ketone (PEEK) tubing was used for the larger ID microchannels while PEEK and PEEKsil™ was used for the smaller ID microchannels.

Table 1 SEM/AUTOCAD estimated microchannel internal diameters

Nominal ID (μm)	Estimated ID (μm)		
	316 stainless steel	PEEK	PEEKsil™ (fused silica)
1000	1008	985	NA
750	787	780	NA
500	511	523	NA
250	250	270	NA
180	158	149	NA
150	NA	123	142
125	114	134	NA
100	NA	103	95
75	NA	80	73

The published tolerances on the IDs of the microchannels are relatively large for the stainless steel and PEEK materials. To obtain a more accurate estimate, the microchannel ends were measured using a SEM and a toolmakers microscope. Images taken from the SEM were imported into AUTOCAD software where they were analyzed using the AREA command, which provided the area and perimeter of the microchannel opening. These values were used to compute the hydraulic diameter, which is a ratio of the area to the perimeter of noncircular channels, to provide a diameter value that can be used to determine Reynolds numbers or pressure losses. The hydraulic diameter is given by

$$d_h = \frac{4A}{p} \tag{1}$$

where A is the cross-sectional area and p is the perimeter of the channel opening. The estimated diameters of the microchannels based on this method are listed in Table 1.

The experiments were conducted by driving the flow of MRG through the different microchannels while measuring the pressure drop. DC currents were varied between 0, 0.25, 0.5, 1, and 2 A through the electromagnet to study how the pressure drop increases with increasing magnetic fields. The strength of the magnetic field in the 1.6 mm (1/16 in.) gap of the electromagnet was measured in air, using an F. W. Bell model 5080 Gauss teslameter. These measurements are shown in Table 2.

For the experiments, the BASF HQ micropowder was mixed into the base grease with 80% weight solids loading. This solid loading is comparable with that of the Lord MRF-132AD. The resulting MRG was loaded into the syringe pump using a second disposable syringe or a grease gun connected to the inline tee before the pressure transducer. The pressure drop measurements were recorded using one of two methods.

(1) For the larger diameter channels, the pump was programmed with step changing flow rates at 10–30 s dwell intervals. As the MRG was dispensed, the pressure drop was recorded with no magnetic field applied to the test microchannel for baseline data, and then the test was run again at each of applied magnetic fields listed in Table 2. Figure 2 shows an example of the data collected using this method.
(2) For the smaller diameter microchannels, the syringe pump was set to deliver a constant flow rate. The pressure drop was monitored on the DAQ computer with no magnetic field applied and when the pressure drop reached a stable reading (constant pressure drop) data storage was initiated and the magnetic field was applied to the microchannel while the increase in pressure drop was recorded. Then, the field was removed and the process was repeated for a different magnetic field strength. An example of the data collected using this method is shown in Fig. 3. This test method was necessary because of the relatively long response time at the small flow rates required while testing the microchannels.

Table 2 Measured magnetic field versus input electric current

dc (A)	Measured magnetic field (T)
0.25	0.19
0.5	0.32
1.0	0.45
2.0	0.56

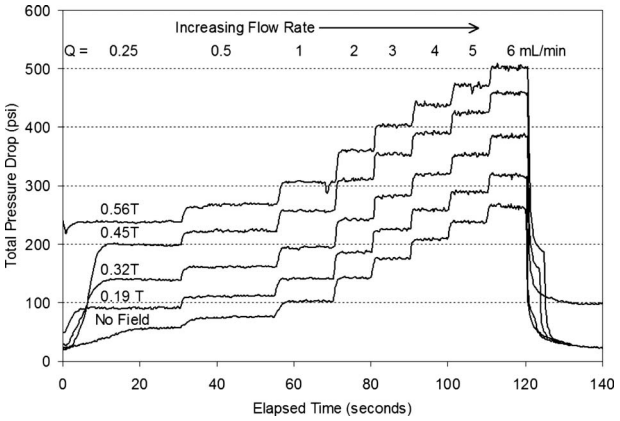

Fig. 2 Raw pressure drop data recorded for 511 μm ID stainless steel channel for step changing flow rate at different applied magnetic fields

3 Results and Discussion

Using a shear rheometer with the plate-plate measurement method, the shear stress can be measured as a function of the applied shear rate for different magnetic field strengths, as shown in Fig. 4. Two theoretical constitutive models are typically used for non-Newtonian fluids that can hold shear; namely, the Bingham plastic and Herschel–Bulkley models. The general form of these models is given in Eqs. (2) and (3) as follows [3]:

$$\tau_{rz} = \tau_y + \eta \left| \frac{du}{dr} \right| \tag{2}$$

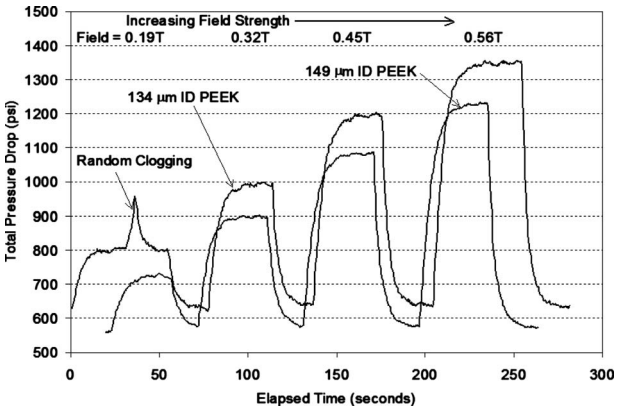

Fig. 3 Raw pressure drop data recorded for PEEK microchannels with a constant MRG flow rate of 0.125 ml/min

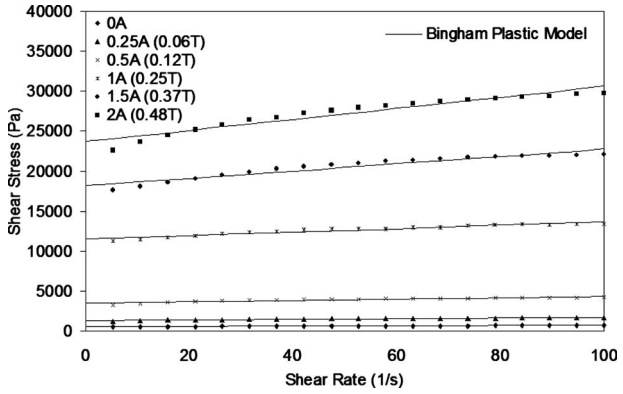

Fig. 4 Shear stress versus shear rate for the MRG using a plate-plate measurement method

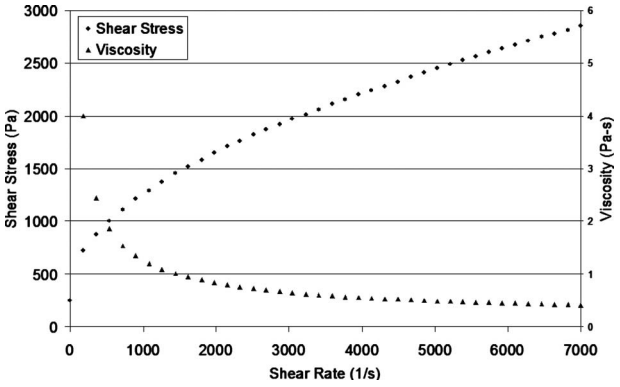

Fig. 6 Shear stress and viscosity versus shear rate for UNR MRG with no magnetic field applied using a cone-plate measurement method

$$\tau_{rz} = \tau_y + k\left|\frac{du}{dr}\right|^n \tag{3}$$

where τ_{rz} is the shear stress, τ_y is the shear yield stress, du/dr is the shear rate, and η is the plastic viscosity for the Bingham model. k and n are fluid index parameters for the Herschel–Bulkley model. In both Equations du/dr is 0 when $\tau_{rz} \leq \tau_y$. The shear yield stress as a function of the applied magnetic field can be obtained by extrapolating a curve of the data points in Fig. 4 using either of these two models to the intersection of the Y axis where the shear rate is zero.

Using the Bingham model in Eq. (2), the values for the shear yield stress were calculated and plotted for comparison against the values for the Lord MRF-132AD fluid as a baseline. The results in Fig. 5 indicate that the MRG has a shear yield stress approximately 25% less than that of the MRF-132AD for a given applied magnetic field. This is expected since the iron particles in the MRG are approximately three times smaller than those in the MRF-132AD; therefore, a smaller magnetic attraction force between particles is generated when the magnetic field is applied.

The total pressure drop for an MRF flowing through a channel is often approximated by

$$\Delta P = \Delta P_{\text{vis}} + \Delta P_{\text{MR}} = \frac{128\eta QL}{\pi D^4} + \frac{c\tau_y L}{D} \tag{4}$$

where ΔP_{vis} is the viscous pressure drop component, and ΔP_{MR} is the pressure drop due to the shear yield component induced by the applied magnetic field. D is the diameter of a circular channel, Q is the volumetric flow rate, and η is the plastic viscosity with an applied magnetic field, which is equivalent to a Newtonian fluid viscosity for MR fluid with no magnetic field applied. L is the channel length, and c is a parameter that ranges between 2 and 3, depending on the ratio of $\Delta P_{\text{MR}}/\Delta P_{\text{vis}}$ [11]. Equation (4) is valid if the MRF behaves as a Newtonian fluid in the absence of a magnetic field as indicated by the Hagen–Poiseuille ΔP_{vis} term on the right for the pressure drop of laminar flow through a pipe. From the results of the MRG under a cone-plate shear rheometer measurement shown in Fig. 6, it is observed that the MRG has a non-Newtonian behavior in the off-state; thus, the ΔP_{vis} term in Eq. (4) would not be appropriate to model the viscous pressure drop.

By comparing the change in pressure drop with the change in flow rate one can determine if one of these models are appropriate to characterize the base grease. In Fig. 7, it can be seen that the data points for each microchannel diameter closely approximate a straight line representing the plastic viscosity η in Eq. (2). This demonstrates that the flow behavior of the base grease material through microchannels still conforms to the macroscale Bingham pipe flow theory.

When the magnetic field is applied along the microchannel, there is approximately 6 mm (0.24 in.) of length that will be influenced by the field, as shown in Fig. 8. This includes the fringing effects of the magnetic field through the gap in the magnet poles, which has an estimated effect out to 1/2 the gap width around the perimeter of the poles. To obtain a qualitative comparison of the influence that the applied magnetic field has on the microchannel pressure drop, the pressure drop due to the viscous portion of the MRG flow that is outside of the 6 mm area of

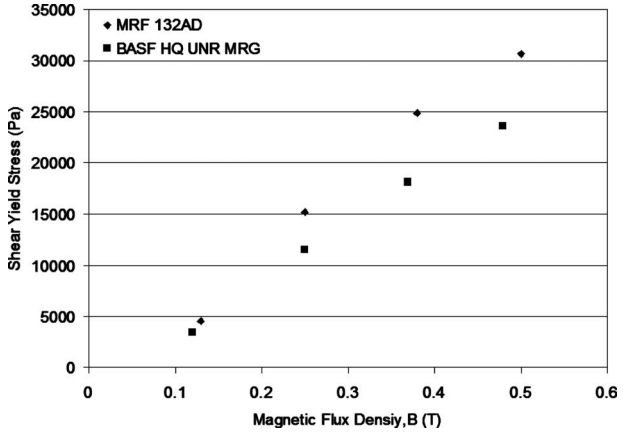

Fig. 5 Shear yield stress versus applied magnetic field for comparing MRG to Lord MRF-132AD using the Bingham model

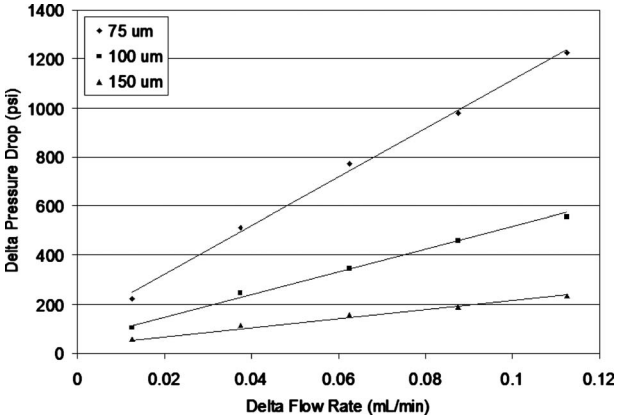

Fig. 7 Change in pressure drop versus change in flow rate in PEEKsil microchannels for the base grease

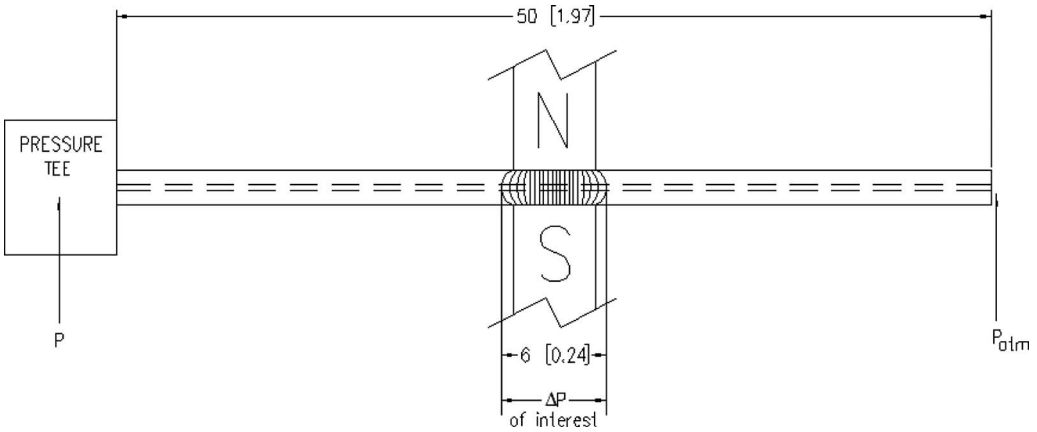

Fig. 8 Approximate length of influence from the magnetic field compared with the total microchannel length. Dimensions are in millimeters (inches).

influence is subtracted from the total pressure drop that was measured. This was accomplished by multiplying the total viscous pressure drop measured, when no magnetic field was applied, by the ratio of the 6 mm active field length to the 50 mm total length of the microchannel. This value was then subtracted from the total pressure drop measured at the same constant flow rate for the different magnetic field strengths applied. The remaining pressure drop was then divided by 6 mm to obtain an average pressure gradient (dp/dz) versus flow rate for the length of microchannel through the applied field.

A theoretical expression has been developed using the Herschel–Bulkley Eq. (3), in combination with the momentum equation for laminar flow [12]

$$r\frac{dp}{dz} = -\frac{\partial(r\tau_{rz})}{\partial r} \tag{5}$$

and the equation for volumetric flow rate in circular channels

$$Q = 2\pi\int_{R_p}^{R} urdr + R_p^2\pi u_p \tag{6}$$

where R is the radius of the channel, u is the flow velocity in the channel, and R_p and u_p are the radius and velocity of the fluid plug that develops for non-Newtonian fluid flow in circular cross sections, respectively. A representation of this geometry and nomenclature is shown in Fig. 9.

By expanding Eqs. (5) and (6) through nondimensional analysis and Taylor series expansions, a closed-form expression of the Herschel–Bulkley constitutive model for the pressure gradient in circular cross sections is found as follows [12]:

$$\frac{dp}{dz} = A\frac{4\tau_y}{D} + \left(\frac{3n+1}{n}\frac{8Q}{\pi D^3}\right)^n\frac{4k}{D}, \quad \frac{R_p}{R} \le 0.5 \tag{7}$$

where

$$A = \frac{3n+1}{2n+1} - \frac{3}{16}\frac{(3n+1)(1-n)}{(2n+1)^2(n+1)}$$

Equation (7) is used to model the dp/dz data obtained by the experiments. The values for τ_y, n, and k can be obtained by from the experimental data. The Levenberg–Marquardt algorithm is commonly used for this type of problem to minimize the sum of the squares between the measured data and the model as follows:

$$F = \sum_{i=1}^{m}\left(\frac{dp}{dz}_{\text{measured}} - \frac{dp}{dz}_{\text{theory}}\right)^2 \tag{8}$$

The *genfit* function in MATHCAD uses this algorithm and was utilized for the process of obtaining results by manually adjusting n to find the set of values for τ_y and k to fit each microchannel tested. The results are shown in Figs. 10–23. In some cases, the best fit curve resulted in a negative value for τ_y. Since this is not physically possible, the value for n was adjusted to provide positive values for τ_y that are reasonable, when compared with the results from the plate-plate shear rheometer in Fig. 4. The values for the parameters in Eq. (7) are presented in Table 3.

The results from Figs. 10–23 indicate that the flow can be modeled using the Herschel–Bulkley model in Eq. (7) with good results. This also indicates that the MRG flow still follows the con-

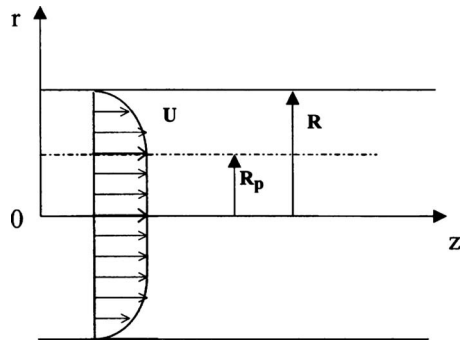

Fig. 9 Flow of MR suspension through a circular cross section [3,13]

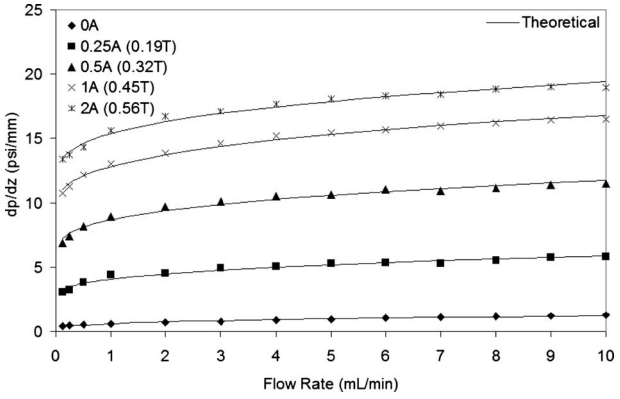

Fig. 10 Pressure gradient versus flow rate across 1008 μm stainless steel microchannel

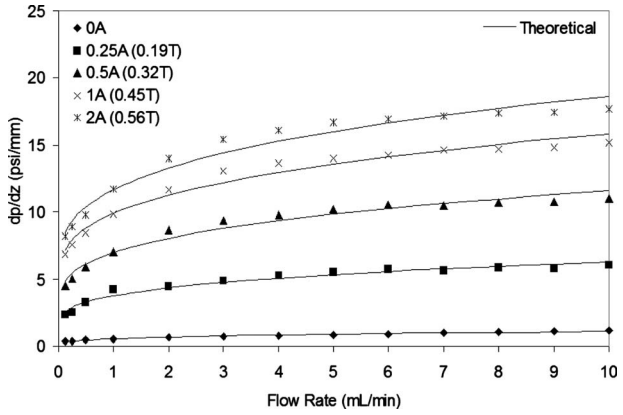

Fig. 11 Pressure gradient versus flow rate across 985 μm PEEK microchannel

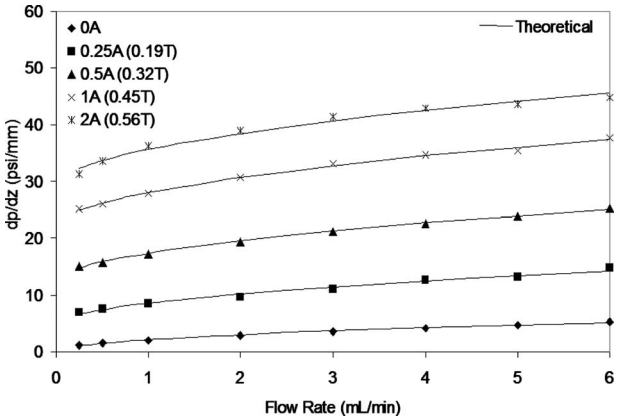

Fig. 14 Pressure gradient versus flow rate across 511 μm stainless steel microchannel

tinuum mechanics law at least down to this microscale tested. For most of the pressure drop results presented, it can be seen that the theoretical approximations using the parameters in Table 3 best match the experimental data for the off-state and the on-states with smaller applied magnetic fields. Slight deviation can be seen at the higher applied magnetic fields. Additionally, deviations are seen at the smaller flow rates for the tests, especially with the PEEK microchannels. By changing the value of the fluid index parameter n for different applied magnetic fields, the model could provide a better approximation of the experimental data for both regions.

The parameter n gives us a measurement of the shear thinning in post yield for a particular fluid with a yield stress. The overall shear thinning effect can be seen in Fig. 6, where the viscosity decreases as the shear rate increases. If $n=1$, then the Herschel–Bulkley model collapses to the Bingham model, in which there is no shear thinning effect after yield. If $n>1$, then the fluid exhibits a shear thickening effect, or an increase in viscosity with increas-

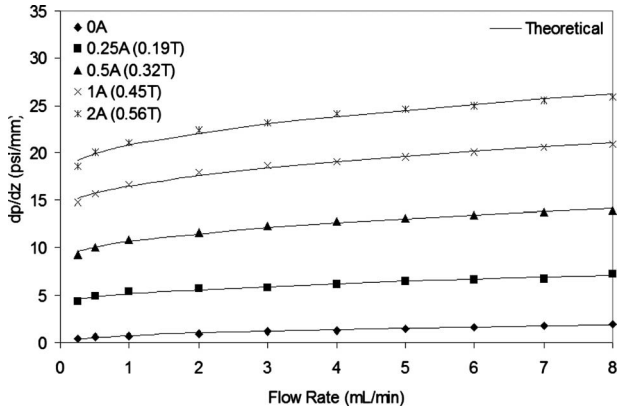

Fig. 12 Pressure gradient versus flow rate across 787 μm stainless steel microchannel

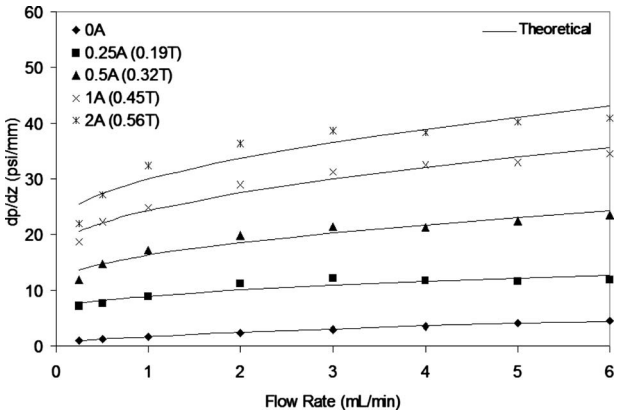

Fig. 15 Pressure gradient versus flow rate across 523 μm PEEK microchannel

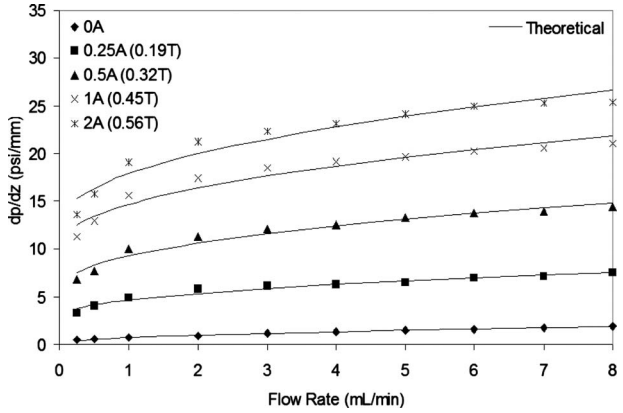

Fig. 13 Pressure gradient versus flow rate across 780 μm PEEK microchannel

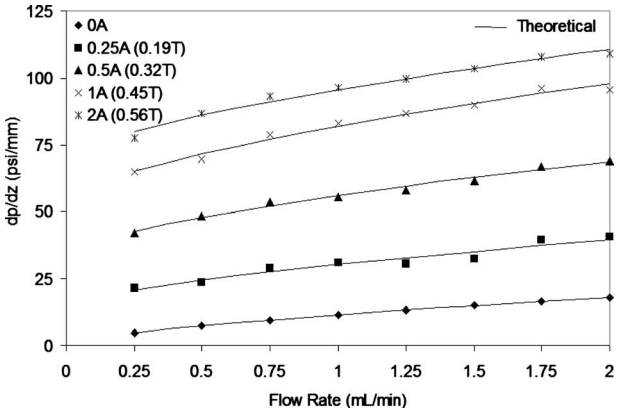

Fig. 16 Pressure gradient versus flow rate across 250 μm stainless steel microchannel

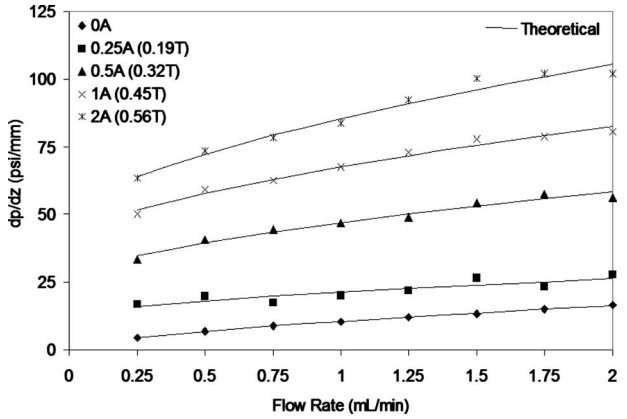

Fig. 17 Pressure gradient versus flow rate across 270 μm PEEK microchannel

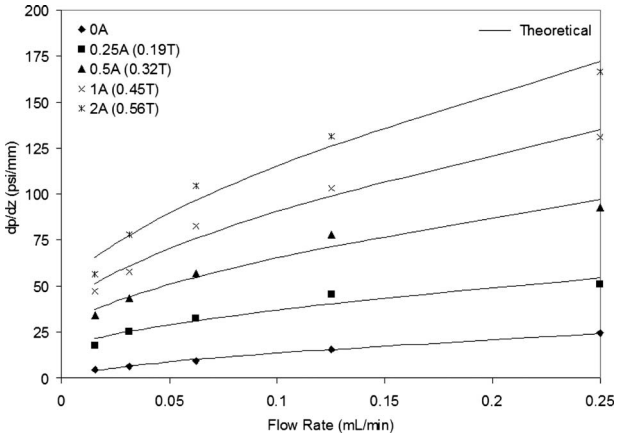

Fig. 20 Pressure gradient versus flow rate across 142 μm PEEKsil™ microchannel

ing shear rate in post yield. In Table 3, it is shown that the general tendency is that n increases as the microchannel diameter decreases. Most likely this is due to the fact that the MRG flow rate range, in the smaller diameter microchannels, does not cover a large of a span as with the larger channels. This is due to the limitations of the experimental setup with regards to maximum working pressure and force ratings on the components.

The dynamic force range or dynamic pressure drop range is often used to characterize the performance of the MR effect in a device. The dynamic pressure drop range is presented graphically in Figs. 10–23, as the area between the pressure gradient results when the magnetic field is applied and at the off-state curve with no magnetic field. The dynamic pressure drop can also be measured by a ratio of the pressure drop due to the MR effect ΔP_{MR} to the pressure drop due to the viscous component ΔP_{vis} mentioned in Eq. (4). From the experimental data, there are two points that can be concluded. The first is that the ratio of $\Delta P_{\mathrm{MR}}/\Delta P_{\mathrm{vis}}$ decreases with increasing flow rate. This is illustrated by comparing measurements on the right side of the figures to those on the

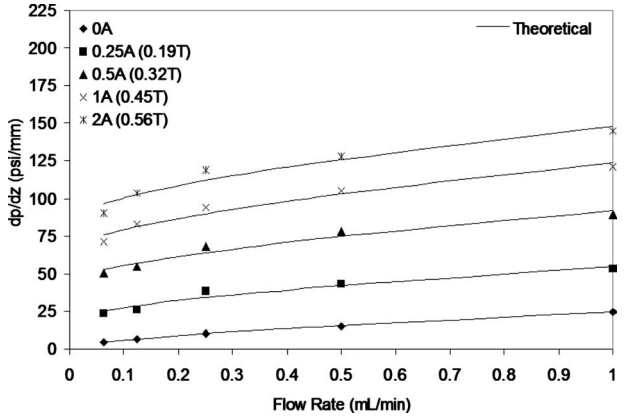

Fig. 18 Pressure gradient versus flow rate across 158 μm stainless steel microchannel

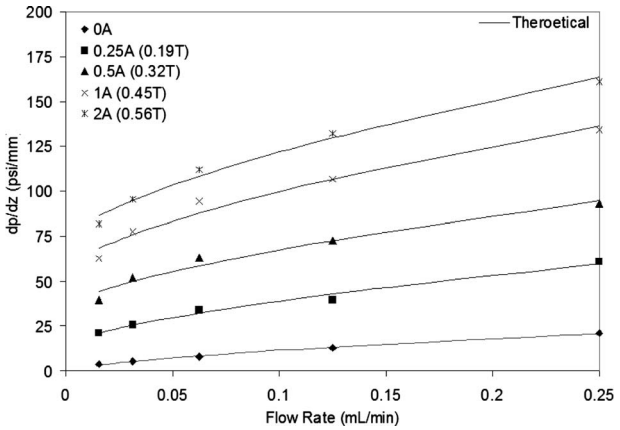

Fig. 21 Pressure gradient versus flow rate across 134 μm PEEK microchannel

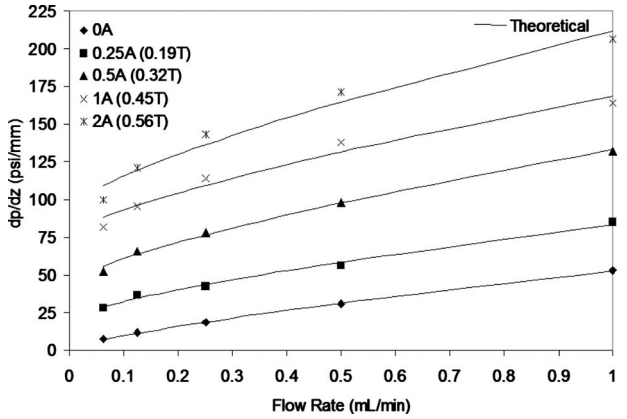

Fig. 19 Pressure gradient versus flow rate across 149 μm PEEK microchannel

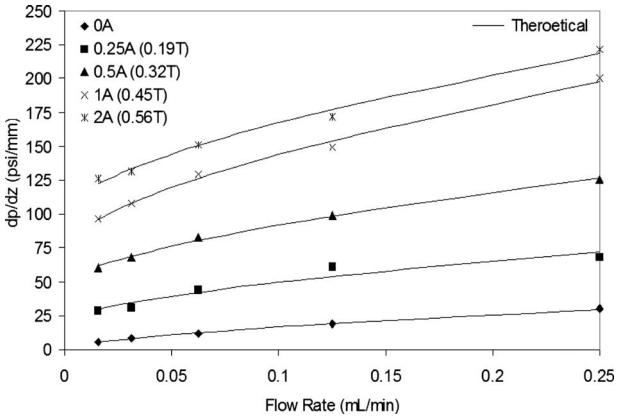

Fig. 22 Pressure gradient versus flow rate across 114 μm stainless steel microchannel

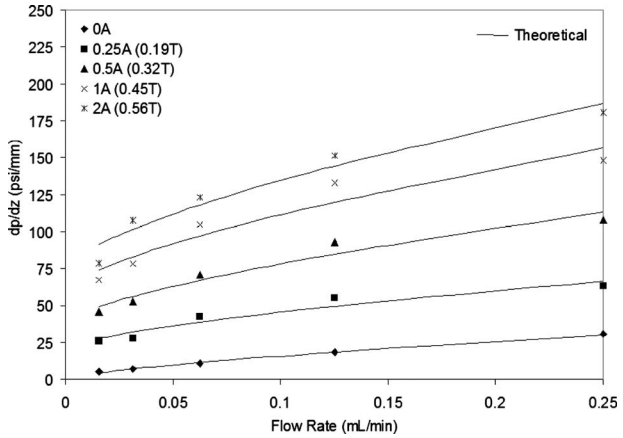

Fig. 23 Pressure gradient versus flow rate across 123 μm PEEK microchannel

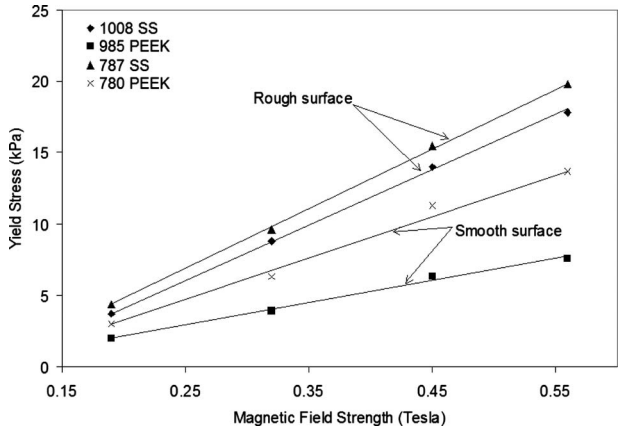

Fig. 24 Yield stress versus magnetic field strength for large stainless steel and PEEK channels

left for the same set of measurement data. In the latter case, $\Delta P_{MR}/\Delta P_{vis}$ is approximately two times greater. Second, $\Delta P_{MR}/\Delta P_{vis}$ decreases with decreasing microchannel diameter. This can be probably explained by an increasing effect of the viscous forces, and a decreasing MR effect at the smaller microchannels due to the reduction in the active fluid volume. The ratio of $\Delta P_{MR}/\Delta P_{vis}$ ranges from about 5, in the smaller microchannels at the highest flow rates, to 30, in the larger channels with the lowest flow rates tested. It is worthy to note that all these phenomena of the MRG flow through microchannels in the tested ranges can be explained well by Eqs. (4) and (7), which are derived from continuum mechanics models.

It has been shown that the surface roughness has significant effect on the flow of MRF [13]. In general, by increasing the surface roughness in a channel, the measured pressure drop of MRF flow will increase for a given applied magnetic field. By using a modified Mason number (a ratio of the viscous forces to magnetic forces) in combination with the friction factor, an expression has been developed that can be used to express the pressure drop for various surface roughness values [13].

Ideally, this would be studied by the pressure drop for microchannels with the same diameter. Because the measurements of the microchannel diameters tested show a significant difference between them for different materials, it is difficult to study the surface roughness effect. In this study, through careful processing of the experimental data, the problems related to the measurement variations in the microchannels and pressure drops were overcome. As stated previously, the hydraulic diameter has been introduced to represent the irregular shape of the microchannels, and a Herschel–Bulkley macroscale pipe flow theory is also employed to utilize the experimental data to obtain the model parameters.

Figures 24 and 25 present the shear yield stress from Table 3 as a function of the applied magnet field for some of the large and smaller microchannels. Values for both stainless steel (rough) and PEEK (smooth) material types are shown for comparison. In Fig. 24, the results indicate that the PEEK channels with their relatively smooth surface roughness have a smaller shear stress than that of the corresponding stainless steel channels. This is consistent with the previous findings [13]. In Fig. 25, the effect of the surface roughness on the smaller diameter microchannels is not easy to discern. The stainless steel and PEEK materials have a shear yield stress that is within the margin of error for the measurements. The PEEKsil™ microchannel exhibits a yield stress that is roughly half the value of the yield stress of the other two materials at the maximum applied magnetic field. These figures suggest that surface effects may diminish as the microchannels get smaller. This may be related to a decreasing MR effect for the smaller active fluid volume, or the increasing viscous forces acting on the fluid. Additionally, these results could be dependent on the fluid properties of the MRG.

The fitted experimental data for the MRG flowing in microchannels using Herschel–Bulkley model include three parameters (n, k, and τ_y). Among the three parameters, the yield stress τ_y is crucial in modeling the MR material flow when subjected to an applied magnetic field. Therefore, the fitted value of the yield stresses are compared with that of the yield stress obtained using

Table 3 Herschel–Bulkley parameters for various microchannels tested

Channel ID (μm)	n	τ_y (kPa)				k (Pa s^n)				
Applied field (T)		0.19	0.32	0.45	0.56	0	0.19	0.32	0.45	0.56
1008 SS	0.31	3.7	8.8	14.0	17.8	191	552	955	1236	1263
985 PEEK	0.31	2.0	3.9	6.3	7.6	159	720	1313	1694	1986
787 SS	0.46	4.4	9.6	15.5	19.8	59.3	103	186	242	286
780 PEEK	0.44	3.0	6.3	11.3	13.7	65.3	176	356	425	521
511 SS	0.51	3.4	8.9	15.8	21.0	42.7	79.0	106	129	137
523 PEEK	0.52	4.8	8.3	12.6	15.9	35.9	50.4	105	150	173
250 SS	0.65	4.9	11.5	18.3	23.6	10.8	15.2	21.1	26.7	25.0
270 PEEK	0.64	4.5	9.7	14.9	18.1	14.2	12.2	28.0	36.9	49.6
158 SS	0.64	4.1	9.6	14.4	18.7	6.6	9.6	12.9	15.6	16.8
149 PEEK	0.74	4.2	8.9	15.3	18.9	4.1	5.0	7.0	7.3	9.3
142 PEEKsil™	0.64	2.8	4.9	6.6	8.4	12.2	20.2	36.3	51.1	65.2
134 PEEK	0.67	2.5	6.4	10.2	13.1	6.6	14.7	19.2	25.7	29.4
114 SS	0.64	3.2	7.5	11.7	16.0	7.9	13.8	21.0	32.8	31.0
123 PEEK	0.69	3.5	6.4	10.0	12.5	5.8	8.9	14.5	18.7	21.7

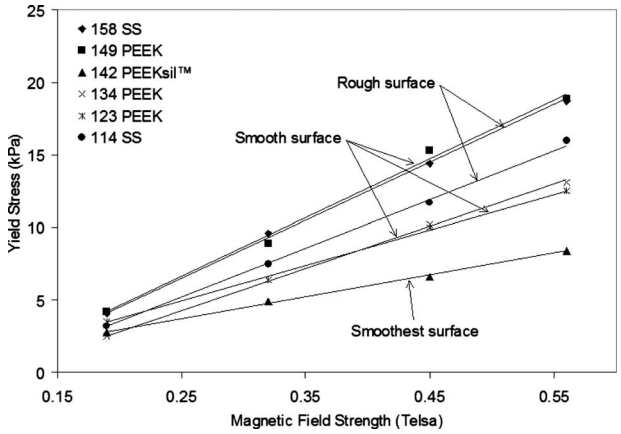

Fig. 25 Yield stress versus magnetic field strength for small stainless steel, PEEK, and PEEKsil™ microchannels

a shear rheometer. These yield stresses, for the MRG, are obtained conventionally by extrapolating a curve of the data points in Fig. 4 using either of Bingham or Herschel–Bulkley models to the intersection of the *Y* axis where the shear rate is zero. The comparisons are only performed on the MRG flow through the stainless steel microchannels, because the surface roughness would affect the measured yield stress, significantly, as it is found in this research. Figure 26 compares the fitted value of the yield stresses using Eq. (7) for microchannel flow with the yield stresses obtained from conventional shear rheometers. It can be seen that the fitted values of yield stresses of MRG flowing through microchannels with a diameter ranging from 114 μm to 1008 μm are all lower than the fitted values obtained from classical rheological techniques. The reason for this could be the slippage of MRG flow at the surface of the microchannels.

In the study of the microchannels with IDs that are 150 μm and smaller, random clogging would occur. Although, not as severe, random clogging also happened for the base experimental grease with no iron micropowders, which was used to generate Figs. 6 and 7. This random clogging is not necessarily due to the same mechanism as a commercial MRF not flowing through the microchannel. In the case of the latter, the MRF would not flow at all through the microchannels or would consistently get clogged just after flow initiation, depending on the microchannel diameter.

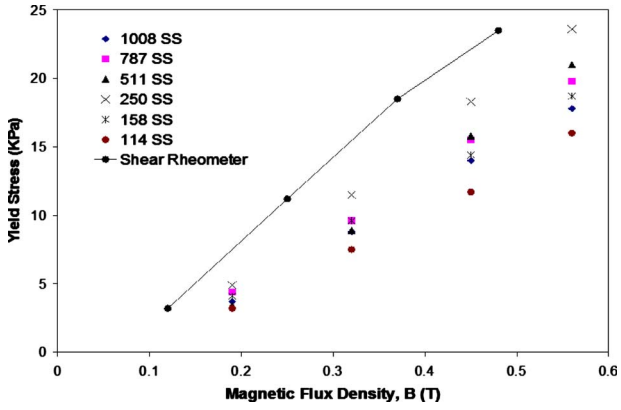

Fig. 26 Comparison of the fitted value of the yield stresses using Eq. (7) for microchannel flow with the yield stresses obtained from parallel-plate shear rheometer under various magnetic fields

With the MRG, flow could be initiated and then random clogging would occur, during either the off or the on (magnetic field applied) states. It is believed that the clogging could be due to one of several phenomena, including:

- contamination from dust, lint, and other foreign matter in the MRG
- structured particle formation within the microchannel forming a wall or dam to block the flow
- particle-particle interaction at the entrance or along the microchannel
- inadequate mixing of the base grease and/or the base grease with the carbonyl iron micropowders

During measurements of the pressure drop for the base grease, all of the clogging that occurred eventually broke free as the pressure increased and steady flow resumed. While this may also be the case with the MRG, the pressures typically approached the 5000 psi limit of the pressure transducer and for safety concerns, the syringe pump was stopped. Then, the microchannel was removed and unplugged by forcing air through it in the opposite direction with a disposable syringe. The random clogging can occur at any location along the microchannel. In lieu of forcing air through the microchannel, there were some cases in which the blockage was able to be removed by bringing a permanent magnet near the entrance or exit of the microchannel. An MRG with the same constituents, but with a 40% solids loading, was tested in the smallest microchannels and the random clogging still occurred.

The compressibility of the MRG is another important issue. The typical response time for a macroscale MRF device is on the order of a few milliseconds. As can be seen in Fig. 3, the response time in these microchannels ranges between 20 s and 30 s for the flow rate shown. The response time decreases with increasing flow rate. When the syringe pump is first initiated, there is a similar lag time during which the flow from the exit of the microchannel gradually increases until the pressure reaches a steady state value. A similar phenomenon is seen when the magnetic field is applied. A reduction in flow rate is observed as the pressure drop builds to a new steady state value. When the field is removed, the pressure drop gradually returns to the steady, off-state value, as seen in the figure. Notice that for the raw data from MRG flow through the 511 μm stainless steel channel in Fig. 2, the response time is much faster, on the order of 1–3 s. It is suspected that these observations are due largely to air that is trapped in the system. Careful precautions were taken to fill individual pieces of the experimental setup with the MRG, as they were assembled to prevent this from occurring. However, the act of transferring the MRG from one container to the grease gun or to another part of the fluid handling system can introduce air that cannot be easily removed.

4 Summary and Conclusions

A method and an apparatus were designed and built to experimentally test the pressure drop of field-controllable fluid flow through microchannels. The setup allows for different commercially available capillaries or microchannels to be attached to it. The syringe pump can be loaded with any type of liquid based MR suspension that is to be studied. Possible future applications for this research include an MR microvalve, microfludic sensors, MR micropumps, and other MEMS based MR devices.

A major challenge of this study revolved around finding a MR suspension that would both flow through microchannels and provide a significant MR effect. The solution to this problem was found in the base carrier medium used to prepare the MR suspension, which in this case was a PAO-based grease with organic clay added as a thickening agent. Commercially available carbonyl iron micropowders with average particle sizes of 1.1 μm were mixed with the base grease to create a MR suspension with 80% solids loading.

The pressure drop of the flow for this MRG was measured across microchannels that were 5 cm in length with nominal internal diameters ranging from 1 mm to 75 μm. A magnetic field was applied midway along the microchannels by an electromagnet. The applied magnetic field strength was varied between four different values from 0.19 T to 0.56 T to study the increase in pressure drop due to the MR effect on the flow. The results indicate that there is good agreement between the experimental data and the macroscale theory, using the Herschel–Bulkley model for flow through a circular cross section. The microchannel materials included stainless steel, PEEK, and fused silica with different values for surface roughness. It was observed that the effect of the surface roughness on the pressure drop diminishes as the microchannel diameter decreases.

Acknowledgment

The authors are thankful for the funding provided by the National Science Foundation. The assistance from the Polymer Science and the Material Science and Engineering students at the University of Nevada, Reno for sample preparation is warmly appreciated.

References

[1] Yoshida, K., Kikuchi, M., Park, J.-H., and Yokota, S., 2002, "Fabrication of Micro Electro-Rheological Valves (ER Valves) by Micromachining and Experiments," Sens. Actuators, A, **95**, pp. 227–233.

[2] Klein, J., and Guckel, H., 1998, "High Winding Density Micro Coils for Magnetic Actuators," Microsyst. Technol., **4**, pp. 172–175.

[3] Wang, X., and Gordaninejad, F., 2007, "Magnetorheological Materials and Their Applications: A Review," *Intelligent Materials*, M. Shahinpoor and H.-J. Schneider, eds., Royal Society of Chemistry, Cambridge, UK, pp. 339–385.

[4] Papautsky, I., Ameel, T., and Frazier, A. B., 2001, "A Review of Laminar Single-Phase Flow in Microchannels," *Proceedings of the ASME International Mechanical Engineering Congress and Exposition*, New York, NY, Nov. 11–16, pp. 1–9.

[5] Judy, J., Maynes, D., and Webb, B. W., 2002, "Characterization of Frictional Pressure Drop for Liquid Flows Through Microchannels," Int. J. Heat Mass Transfer, **45**, pp. 3477–3489.

[6] Sharp, K., and Adrian, R., 2001, "Shear-Induced Arching of Particle-Laden Flows in Microtubes," *ASME IMECE2001/MEMS-23879*, Vol. 2, ASME, New York.

[7] Kormann, C., Laun, H. M., and Richter, H. J., 1996, "MR Fluids With Nano-Sized Magnetic Particles," Int. J. Mod. Phys. B, **10**, pp. 3167–3172.

[8] Liu, J., Flores, G. A., and Sheng, R., 2001, "In-Vitro Investigation of Blood Embolization in Cancer Treatment Using Magnetorheological Fluids," J. Magn. Magn. Mater., **225**, pp. 209–217.

[9] Haghgooie, R., Li, C., and Doyle, P. S., 2006, "Experimental Study of Structure and Dynamics in a Monolayer of Paramagnetic Colloids Confined by Parallel Hard Walls," Langmuir, **22**, pp. 3601–3605.

[10] Sinha, K., 2005, "Large Scale Synthesis of Crystalline Magnetic Nanoparticles," MS thesis, Material Science and Engineering Department, University of Nevada, Reno.

[11] Carlson, J. D., Catanzarite, D. N., and St Clair, K., 1996, "Commercial Magneto-Rheological Fluid Devices," *Proceedings of the 5th International Conference on Electro-Rheological Fluids, Magneto-Rheological Suspensions, and Associated Technology*, W. Bullough, ed., World Scientific, Singapore, pp. 20–28.

[12] Wang, X., and Gordaninejad, F., 1999, "Flow Analysis of Field-Controllable, Electro- and Magneto-Rheological Fluids Using Herschel-Bulkley Model," J. Intell. Mater. Syst. Struct., **10**(8), pp. 601–608.

[13] Gordaninejad, F., Kavlicoglu, B., and Wang, X., 2005, "Friction Factor of Magneto-Rheological Fluid Flow in Grooved Channels," Int. J. Mod. Phys. B, **19**(7–9), pp. 1297–1303.